NASA TN D-1816

TECHNICAL NOTE

D-1816

COMPARISON OF STEADY-STATE AND SIX-DEGREE-OF-FREEDOM ANALYSES OF PITCH-ROLL RESONANCE CONDITIONS FOR A LONG SLENDER SOUNDING ROCKET

By Charles H. Whitlock

Langley Research Center
Langley Station, Hampton, Va.

NATIONAL AERONAUTICS AND SPACE ADMINISTRATION
WASHINGTON June 1963

Table 1

NATIONAL AERONAUTICS AND SPACE ADMINISTRATION

TECHNICAL NOTE D-1816

COMPARISON OF STEADY-STATE AND SIX-DEGREE-OF-FREEDOM ANALYSES OF PITCH-ROLL RESONANCE CONDITIONS FOR A LONG SLENDER SOUNDING ROCKET

By Charles H. Whitlock

SUMMARY

The amplitude response of a long slender sounding rocket under pitch-roll resonance conditions has been computed by two methods: a six-degree-of-freedom method of analysis and an approximate solution assuming steady-state flight conditions. Resultant flow incidence angles and principal vehicle structural loadings were calculated by both methods and compared throughout a typical flight. From this comparison it is concluded that the steady-state method of analysis was useful in determining and understanding the loading conditions imposed by pitch-roll resonance for the model and trajectory in question.

INTRODUCTION

Within the aerospace industry it is recognized that there are many problems concerning the ascent phase of unguided rocket flight which are caused by rapidly changing vehicle velocities and altitudes. It is generally accepted that one of the more important of these problems is that of both the nutational and roll frequencies of the rocket vehicle being equal at some instant of flight time. In the case of long slender vehicles, the nutational frequency is almost equal to the natural pitch frequency; hence, this condition has become known as pitch-roll resonance. This condition creates a coupling of vehicle motions which in turn may cause the total angle of attack to become quite large, ultimately leading to structural failure of the vehicle. The severity of this condition is mainly a function of vehicle asymmetries, aerodynamics, inertia, and response time, all near the instant of pitch-roll resonance. The fact that condition severity is dependent upon the magnitudes of these quantities causes pitch-roll resonance to be a problem which must be studied during the preliminary design phase of any missile configuration.

The first step in the analysis of pitch-roll resonance conditions is one of calculating the basic aerodynamics and physical properties of the system in question. From this, vehicle motions due to the condition may be approximated by steady-state calculations as given in references 1, 2, and 3. Presently there

is a need for a basic knowledge of the degree of accuracy by this method of analysis. It is the purpose of this paper to obtain some insight into this problem. In order to do this, the magnitudes of certain vehicle motions and loads will be obtained by two methods: the steady-state type of analysis, already mentioned, and a more accurate six-degree-of-freedom method of calculation, obtained by use of the IBM 7090 electronic data processing system. More specifically, the magnitudes of both the total angles of attack and the principal structural loadings under several pitch-roll resonance conditions, as obtained by the separate methods on the same vehicle, are compared and some conclusions drawn with respect to the accuracy of the steady-state method of analysis.

SYMBOLS

A	body frontal area, sq ft
a,b,c	direction cosine used in computing thrust component along missile X-, Y-, and Z-axis, respectively,
a_X, a_Y, a_Z	accelerations parallel to missile X-, Y-, and Z-axis, respectively, ft/sec^2
$C_{A,0}$	axial-force coefficient at zero flow incidence angle (positive in negative X-direction)
ΔC_A	increment of axial-force coefficient due to flow incidence angle
C_N	normal-force coefficient $(-C_Z)$
C_{N_α}	rate of change of normal-force coefficient with angle of attack, $\frac{\partial C_N}{\partial \alpha}$, 1/radian
C_{N_δ}	rate of change of pitch or yaw normal-force coefficient with fin deflection, $\frac{\partial C_N}{\partial \delta}$, 1/radian
C_l	rolling-moment coefficient
C_{l_p}	rate of change of rolling-moment coefficient with rolling velocity, $\frac{\partial C_l}{\partial\left(\frac{pD}{2V'}\right)}$, 1/radian
C_{l_δ}	rate of change of rolling-moment coefficient with fin deflection, $\frac{\partial C_l}{\partial \delta}$, 1/radian

C_m pitching-moment coefficient

C_{m_q} rate of change of pitching-moment coefficient with pitching velocity, $\frac{\partial C_m}{\partial\left(\frac{qD}{2V'}\right)}$, 1/radian

$C_{m_{\dot{\eta}}}$ rate of change of pitching-moment coefficient with rate of change of flow incidence angle, $\frac{\partial C_m}{\partial\left(\frac{\dot{\eta}D}{2V'}\right)}$, 1/radian

C_n yawing-moment coefficient

C_{n_r} rate of change of yawing-moment coefficient with yawing velocity, $\frac{\partial C_n}{\partial\left(\frac{rD}{2V'}\right)}$, 1/radian

D body diameter, ft

d,e,f moment arm for thrust moment about missile X-, Y-, and Z-axis, respectively, ft

F_N normal force parallel to negative Z-axis, lb

F_{N_α} rate of change of normal force parallel to negative Z-axis with angle of attack, lb/radian

$F_X(t),F_Y(t),F_Z(t)$ force along X-, Y-, and Z-axis, respectively, as a function of time, lb

F_Y force parallel to Y-axis, lb

F_{Y_β} rate of change of force parallel to Y-axis direction with angle of sideslip, lb/radian

g acceleration due to force of gravity, ft/sec^2

I mass moment of inertia about Y- and Z-axes for a symmetric vehicle, slug-ft^2

I_X,I_Y,I_Z mass moment of inertia about X-, Y-, and Z-axis, respectively, slug-ft^2

I_{XZ} product of inertia, slug-ft^2

k radius of gyration, ft

M	moment about vehicle center of gravity, ft-lb
M_X, M_Y, M_Z	moment about X-, Y-, and Z-axis, respectively, ft-lb
$M_X(t), M_Y(t), M_Z(t)$	moment about X-, Y-, and Z-axis, respectively, as a function of time, ft-lb
$\left(M_{X_p}\right)_j$	rate of change of rolling moment with rolling velocity due to jet damping, ft-lb-sec/radian
M_{Y_q}	rate of change of pitching moment with pitching velocity, ft-lb-sec/radian
$\left(M_{Y_q}\right)_j$	rate of change of pitching moment with pitching velocity due to jet damping, ft-lb-sec/radian
M_{Y_α}	rate of change of pitching moment with angle of attack, ft-lb/radian
M_{Z_r}	rate of change of yawing moment with yawing velocity, ft-lb-sec/radian
$\left(M_{Z_r}\right)_j$	rate of change of yawing moment with yawing velocity due to jet damping, ft-lb-sec/radian
M_{Z_β}	rate of change of yawing moment with angle of sideslip, ft-lb/radian
p	rolling velocity, radians/sec
q	pitching velocity, radians/sec
q'	dynamic pressure, lb/sq ft
r	yawing velocity, radians/sec
T	thrust as a function of time, lb
u, v, w	component of missile linear velocity relative to earth along X-, Y-, and Z-axis, respectively, ft/sec
u', v', w'	component of missile linear velocity relative to wind along X-, Y-, and Z-axis, respectively, ft/sec
V	missile linear velocity relative to earth, ft/sec
V'	total missile linear velocity relative to wind, ft/sec
X, Y, Z	body axes of missile
$\bar{x}, \bar{y}, \bar{z}$	distance to center of gravity of point on missile from vehicle center of gravity along X-, Y-, and Z-axis, respectively, ft

x_{cg}	center-of-gravity distance from nose, ft
x_{cp}	center-of-pressure distance from nose with zero fin deflection, ft
$x_{cp,tail}$	tail center-of-pressure distance from nose with fins deflected, ft
x_{sm}	stability margin distance, $x_{cp} - x_{cg}$, ft
α	angle of attack, radians
β	angle of sideslip, radians
δ	fin deflection, radians
δ_p	roll fin deflection (positive for positive rolling moment), radians
δ_q	pitch fin deflection (positive for negative pitching moment), radians
δ_r	yaw fin deflection (positive for negative yawing moment), radians
η	resultant or total flow incidence angle $\left(\alpha^2 + \beta^2\right)^{1/2}$, radians unless otherwise noted
θ	pitch angle of missile relative to earth-fixed axes, radians
ϕ	roll angle of missile relative to earth-fixed axes, radians
ϕ'	roll angle of missile relative to plane defined by V' and X-axis, radians
ψ	yaw angle of missile relative to earth-fixed axes, radians
Ω	total angular velocity of missile, $\dot{\theta} + i\dot{\psi}$, radians/sec
ω	vehicle undamped pitch natural frequency, $\left(-\frac{M_{Y_\alpha}}{I}\right)^{1/2}$, radians/sec

Subscripts:

cg	vehicle center of gravity
max	maximum
o	because of asymmetries
pl	vehicle payload

Dots over symbols denote differentiation with respect to time; $|\ |$ denotes absolute values.

CONFIGURATION

For purposes of analysis, a configuration consisting of a long slender single-stage sounding rocket was chosen as shown in figure 1. The configuration chosen is 96.2 inches long, 4.5 inches in body diameter, and has a span of 13.0 inches. The fins have an exposed area of 0.215 sq ft per panel. The vehicle is assumed to terminate the thrusting phase of flight at 31 seconds and to coast to apogee without change in external configuration. Figure 2 presents estimated values of several aerodynamic parameters plotted against Mach number for the vehicle. Values for C_{N_α}, x_{cp}, $C_{A,0}$, C_{N_δ}, C_{m_q}, C_{l_p}, and C_{l_δ} are given based on both reference area and diameter equal to 1. Figure 3 gives time histories of some estimated physical properties of the vehicle. Values are given for thrust, weight, x_{cg}, $\left(M_{Y_q}\right)_j$, and roll, pitch, and yaw inertias $\left(I_X,\ I_Y,\right.$ and $\left.I_Z,\ \text{respectively}\right)$.

SIX-DEGREE-OF-FREEDOM ANALYSIS

This analysis was carried out by use of the six-degree-of-freedom trajectory program described in reference 4. The basic equations of motion used in this program are shown in appendix A. These equations are referenced to the body axes system, as shown in figure 4, and include (1) the usual rigid-body kinematic terms, (2) gravity terms, (3) aerodynamic forces and moments, (4) damping due to mass movement within the vehicle (usually referred to as jet damping), (5) thrust and fin misalinements, and (6) any other external forces or moments which may be programed as functions of time. The lag in downwash terms $C_{m_{\dot{\eta}}}$ and jet damping in roll are neglected in this investigation.

Positions, motions, and accelerations about the center of gravity of the vehicle are obtained from this program. Knowing these quantities, accelerations on other parts of the vehicle are obtained by the use of the equations shown in appendix B. These equations express the accelerations acting on a point some $\bar{x}$, $\bar{y}$, and $\bar{z}$ distance from the center of gravity of a vehicle rotating with p, q, and r angular velocities.

Use of the six-degree-of-freedom program with estimated aerodynamics and physical properties, allows a basic ascent trajectory for the vehicle to be obtained as shown in figure 5. This trajectory is based on an 80° sea-level launch, no misalinements, and an initial exit velocity of 230 ft/sec from the vehicle launcher. From this figure, it can be noted that the velocity increase is approximately linear during the thrusting phase and that the dynamic pressure is decreasing near burnout.

Combination of the basic trajectory with vehicle aerodynamics and physical properties allows approximate values for the vehicle undamped pitch natural frequency, $\omega = \left(-\frac{M_{Y_\alpha}}{I}\right)^{1/2}$, to be calculated at various flight times by methods presented in reference 3. Figure 6 presents these calculated values of ω. Also shown in this figure are roll (spin) rate histories for those selected, but incidental, vehicle fin deflections in roll to be studied in this analysis. These histories were calculated by approximate steady-state methods as presented in reference 5 and give good agreement with the program results. The maximum control deflection under investigation causes the vehicle to fly near pitch-roll resonance for the first 11 seconds of flight, at which time it traverses the condition, and to produce a maximum roll rate of 100 radians/sec at burnout. The lowest roll input to be studied produces a rate of 15 radians/sec at burnout and causes resonance to occur during coast, at 34 seconds after launch. For the rest of this investigation, the particular spin time history being studied will be referred to by its value of roll rate at burnout. The spin time histories under investigation will be those of 15, 22, 27, 37, 50, 66, 80, and 100 radians/sec as shown in figure 6.

As stated previously, one of the main variables affecting the severity of pitch-roll resonance is that of vehicle asymmetries. For the purposes of this investigation, 0.25° of thrust misalinement, 0.0825° of fin cant, and 0.075° of nose misalinement in the vehicle's yaw plane are assumed to cause the vehicle to deviate from the purely ballistic zero-angle-of-attack trajectory. The moments resulting from these asymmetries being additive cause the vehicle to assume the resultant or total flow incidence angles as shown in figure 7. The values shown on the upper plot of this figure are those of a nonrolling vehicle, whereas the lower plot presents total flow incidence angle time histories for the vehicle rolling at the several different roll rates. In the case of the rolling vehicle, envelopes about both the precessional and nutation motions are presented for reasons of simplicity. These curves were obtained as a result of the six-degree-of-freedom calculations and indicate a sharp increase from the nonrolling trim when the vehicle pitch frequency is comparable in magnitude to its roll frequency. In fact for each roll time history, it should be noted that the flow incidence angle rises sharply, peaks, and falls off to a very low value as the vehicle approaches and passes through pitch-roll resonance. The dashed curve is an envelope faired through the resonant peaks.

An important consideration during the preliminary design of any missile configuration is the magnitude of vehicle loadings during resonance. In most cases there are certain areas and types of loading on the vehicle which are critical and hence subject to intense investigation. Preliminary considerations of transverse loadings and probable vehicle structure indicated that payload and fin environment are the questionable items to be considered on the configuration under study. Preliminary calculations indicate that transverse inertia loadings on the fins are negligible in comparison to aerodynamic loads. The principal payload transverse force, however, is the inertia load. Hence the results given subsequently will be based on transverse aerodynamic fin loads and inertial payload forces.

Use of fin aerodynamics, program results as previously mentioned, and the equations presented in appendix B yield values for the principal vehicle loadings presented in figure 8. Note that the fin loads rise sharply, peak, and fall to low values as pitch-roll resonance is transversed as did the flow incidence angles in figure 7. Thus, the time at which fin loading peaks is also the approximate time at which the vehicle passes through pitch-roll resonance. The case of the forces acting on the payload is not so easy to generalize. Note that at most instances, maximum payload forces occur around resonance. This is not the case, however, when a roll rate of 50 radians/sec is used. Under these conditions, resonance (23 seconds after launch) is where a minimum of payload forces occur. In fact at this particular instant of flight time, payload forces are a minimum for all roll rates. The reason behind this phenomenon will be investigated in the steady-state analysis which follows.

STEADY-STATE ANALYSIS

The steady-state type of dynamic analysis at pitch-roll resonance has been presented in several past publications such as references 1 and 2. For the sake of brevity, only the results of these analyses will be presented in the text of this report. A complete derivation of these results is presented in appendix C, however.

Simplification of the six equations of motion presented in appendix A, along with steady-state assumptions, allows the total or resultant flow incidence angle of a rocket vehicle at pitch-roll resonance ($p = \omega$) to be expressed as shown in the following equation (eq. (C6)):

$$\left|\frac{\eta_{p=\omega}}{\eta_{p=0}}\right| = \frac{\left(-\frac{M_{Y_\alpha}}{I}\right)^{1/2}}{\frac{F_{N_\alpha}}{mV} - \frac{M_{Y_q}}{I}} \qquad \left(\frac{I_X}{I} \ll 1\right) \qquad (1)$$

This equation expresses the total flow incidence angle at resonance in terms of vehicle aerodynamics, mass, inertia, and nonrolling total flow incidence angle at any instant of flight time. By knowing vehicle asymmetries and aerodynamics, the nonrolling total flow incidence angle may be calculated at various instances of flight time. The results of these calculations applied to the configuration under investigation are shown in the upper plot of figure 9. Knowing this, the total flow incidence angles at resonance, at various flight times, may also be calculated from equation (1) and are shown for the test vehicle in the lower plot of figure 9. Also shown in this plot are those results obtained from the six-degree-of-freedom analysis.

Use of the steady-state resonant flow incidence angles at the reaction times given in figure 6 along with fin aerodynamics allows the transverse fin loadings of the vehicle to be calculated. In the case of transverse payload forces, however, the accelerations involved must first be examined. If small perturbation

and complex plane criteria are applied to the equations presented in appendix B, the resulting equation for the accelerations acting on the payload is

$$\left(\frac{a_Y + ia_Z}{g}\right)_{pl} = \left(\frac{a_Y + ia_Z}{g}\right)_{cg} + \frac{\bar{x}}{g}\left[(pq + \dot{r}) + i(pr - \dot{q})\right] \tag{2}$$

But if $\frac{I_X}{I} \ll 1$, $\frac{M_Z - iM_Y}{I}$ may be expressed as follows:

$$(pq + \dot{r}) + i(pr - \dot{q}) = -\frac{x_{sm}}{I}\left(F_Y - iF_N\right) = -\frac{x_{sm}}{k^2} g\left(\frac{a_Y + ia_Z}{g}\right)_{cg} \tag{3}$$

therefore, the following equations are true:

$$\left(\frac{a_Y + ia_Z}{g}\right)_{pl} = \left(\frac{a_Y + ia_Z}{g}\right)_{cg} - \frac{\bar{x}x_{sm}}{k^2}\left(\frac{a_Y + ia_Z}{g}\right)_{cg} \tag{4}$$

or

$$\left(\frac{a_Y + ia_Z}{g}\right)_{pl} = \left(\frac{a_Y + ia_Z}{g}\right)_{cg}\left(1 - \frac{\bar{x}x_{sm}}{k^2}\right) \tag{5}$$

Equation (5) expresses the accelerations on the nose or payload in terms of the accelerations on the vehicle center of gravity and the term $\left(1 - \frac{\bar{x}x_{sm}}{k^2}\right)$. To aid in the understanding of this last term, a plot of its values, as calculated from the assumption of a payload center of gravity at 2.05 feet from the nose and the basic vehicle and trajectory data from figures 2, 3, and 5, is shown in figure 10. This plot indicates that $1 - \frac{\bar{x}x_{sm}}{k^2}$ passes through zero at approximately 22 seconds of flight time. According to equation (5), the accelerations on the nose are zero at 22 seconds no matter how severe those on the center of gravity. Physically this phenomenon can be explained as follows. Any body whose center of gravity has a translatory motion as well as a rotary motion about itself can be considered to be in rotary motion about some instantaneous center of rotation which does not translate. As the stability and center of gravity change during rocket burning, this instantaneous center of rotation moves forward or backward along the longitudinal axis. The factor $1 - \frac{\bar{x}x_{sm}}{k^2}$ expresses the effect of this movement on the acceleration at a particular point $\bar{x}$ corresponding to the payload position. The fact that $1 - \frac{\bar{x}x_{sm}}{k^2} = 0$ at 22 seconds of flight time for the

vehicle in question indicates that at this particular instant of time, the instantaneous center of rotation is on the payload, hence payload transverse forces are zero. If absolute values for $1 - \frac{\bar{x}x_{sm}}{k^2}$ are now used with the assumption that

$$\left|a_Y + ia_Z\right| = \frac{\left|F_{N_\alpha}\right|\eta_{p=\omega}}{m}$$

values for the inertia forces acting on the payload at various pitch-roll resonance times obtained from figure 6, can then be calculated from steady-state results presented in figure 9.

A particular vehicle with various roll time histories has been used throughout this analysis. Because roll rate has been the principal variable in this investigation, more useful information may be derived if the results of the steady-state analysis are shown as a function of this variable. Figure 11 presents the steady-state principal vehicle loadings at resonance plotted against maximum roll rate. Also shown in this figure are the results obtained from the six-degree-of-freedom analysis.

DISCUSSION

From the results of the two methods of analysis presented, several items are of interest. Figure 9 gives some indication of the accuracy obtained in predicting both nonrolling and resonance total flow incidence angles by the steady-state analysis and may be summarized as follows. For a vehicle with zero roll, hence no resonance problem, steady-state approximations are in excellent agreement with six-degree-of-freedom results after the initial phase of flight in which launcher dynamics are appreciable. In the case of the rolling vehicle, however, agreement between the two methods is not as good. During that portion of flight between 10 and 26 seconds, the results appear close although differences, always on the conservative level, begin to result at later flight times. Some of this error may be explained by a fact not immediately apparent from figure 9; that is, the times of pitch-roll resonance as calculated by the steady-state method do not exactly agree with the actual times of resonance as calculated by the six-degree-of-freedom method. Consider, for example, the case in which the vehicle was rolled to a maximum of 50 radians/sec at burnout. From figure 6, the steady-state calculations indicate that pitch-roll resonance will occur near 22 seconds, whereas from figure 7 it actually occurred near 23 seconds. If this particular roll rate is considered and the steady-state resonance angle $\left(\eta_{resonance} = 1.55^\circ \text{ at } 22 \text{ seconds}\right)$ is compared with the six-degree-of-freedom resonance angle $\left(\eta_{resonance} = 1.47^\circ \text{ at } 23 \text{ seconds}\right)$, the difference between the two methods for a particular roll time history is not as great as is first indicated in figure 9. It must be recognized, however, that this difference in time only accounts for a small amount of the total error indicated during the later

flight times. The large inaccuracy under these conditions is probably due to the fact that one of the main variables affecting pitch-roll resonance, that of the time necessary for response, was not taken into account in the steady-state method of analysis. At the higher altitudes, the response time of the vehicle to pitch-roll resonance is large enough that the resonance condition is apparently traversed before the vehicle has time to react.

In the case of the principal vehicle loadings at resonance, presented in figure 11, the agreement between steady-state and six-degree-of-freedom results is good when the vehicle roll history was such that the roll rate at burnout was between 37 and 100 radians per second; hence, pitch-roll resonance was traversed at the lower altitudes. Again the errors are amplified when roll rates between 10 and 37 radians per second and high pitch-roll resonance altitudes are the case.

CONCLUDING REMARKS

From the results presented, several statements may be made with regard to the accuracy obtained when using steady-state methods to determine pitch-roll resonance conditions on the test vehicle. Steady-state approximations gave results which were in good agreement with those obtained as a result of the six-degree-of-freedom analysis when the vehicle spin history was such that the roll rate at burnout was between 37 and 100 radians/sec; hence, pitch-roll resonance was transversed at the lower altitudes. In the case of the lower roll histories, pitch-roll resonance occurring at very high altitudes, agreement between the two methods is poor, however. The major reason for this deviation probably lies in the fact that vehicle response time was not taken into account in the steady-state analysis. Even with this being the case, it is concluded that this method of analysis was useful in determining and understanding the load conditions at pitch-roll resonance for the vehicle in question.

It should be recognized that the vehicle under consideration has a very low roll inertia as compared to its pitch inertia. It is expected that on high roll inertia types of vehicles, agreement would not be as good as that presented here. Because of this and the fact that vehicle response times are not taken into account in the steady-state method of analysis, it must be emphasized that one must be very careful when using data obtained in this manner. In all cases, once final design is complete, the more accurate six-degree-of-freedom analysis is a necessity for final predictions of in-flight vehicle motions and loads.

Langley Research Center,
National Aeronautics and Space Administration,
Langley Station, Hampton, Va., April 9, 1963.

APPENDIX A

SIX-DEGREE-OF-FREEDOM EQUATIONS OF MOTION

The equations of motion associated with six degrees of freedom, as given in reference 4, are given in the notation of the present paper as follows:

$$m(\dot{u} - vr + wq) = F_X(t) + Ta - mg \sin\theta - \left\{C_{A,0} + \Delta C_A\right\} q'A \tag{A1}$$

$$m(\dot{v} - wp + ur) = F_Y(t) + Tb + mg \sin\phi \cos\theta + \left\{-C_N \sin\phi' + C_{N_\delta}\delta_r\right\} q'A \tag{A2}$$

$$m(\dot{w} - uq + vp) = F_Z(t) + Tc + mg \cos\phi \cos\theta - \left\{C_N \cos\phi' + C_{N_\delta}\delta_q\right\} q'A \tag{A3}$$

$$\dot{p}I_X - \dot{r}I_{XZ} + \left(I_Z - I_Y\right)qr - pqI_{XZ} = M_X(t) + Td + \left(M_{X_p}\right)_j p + \left\{C_{l_p}\left(\frac{pD}{2V'}\right) + C_{l_\delta}\delta_p\right\} q'AD \tag{A4}$$

$$\dot{q}I_Y + rp\left(I_X - I_Z\right) + \left(p^2 - r^2\right)I_{XZ} = M_Y(t) + Te + \left(M_{Y_q}\right)_j q + \left\{\left[C_N\left(\frac{x_{cg}}{D} - \frac{x_{cp}}{D}\right) + C_{m_{\dot{\eta}}}\left(\frac{\dot{\eta}D}{2V'}\right)\right]\cos\phi' + C_{N_\delta}\left(\frac{x_{cg}}{D} - \frac{x_{cp,tail}}{D}\right)\delta_q + C_{m_q}\left(\frac{qD}{2V'}\right)\right\} q'AD \tag{A5}$$

$$\dot{r}I_Z - \dot{p}I_{XZ} + \left(I_Y - I_X\right)pq + I_{XZ}qr = M_Z(t) + Tf + \left(M_{Z_r}\right)_j r + \left\{-\left[C_N\left(\frac{x_{cg}}{D} - \frac{x_{cp}}{D}\right) + C_{m_{\dot{\eta}}}\left(\frac{\dot{\eta}D}{2V'}\right)\right]\sin\phi' + C_{N_\delta}\left(\frac{x_{cg}}{D} - \frac{x_{cp,tail}}{D}\right)\delta_r + C_{N_r}\left(\frac{rD}{2V'}\right)\right\} q'AD \tag{A6}$$

APPENDIX B

ACCELERATIONS ACTING AT POINT NOT AT CENTER OF GRAVITY OF VEHICLE

The accelerations at a point not at the center of gravity of the vehicle are given by the following equations:

$$a_X = a_{X,cg} - \left(r^2 + q^2\right)\bar{x} + (pq - \dot{r})\bar{y} + (\dot{q} + rp)\bar{z} \tag{B1}$$

$$a_Y = a_{Y,cg} + (pq + \dot{r})\bar{x} - \left(p^2 + r^2\right)\bar{y} + (-\dot{p} + rq)\bar{z} \tag{B2}$$

$$a_Z = a_{Z,cg} + (pr - \dot{q})\bar{x} + (rq + \dot{p})\bar{y} - \left(p^2 + q^2\right)\bar{z} \tag{B3}$$

APPENDIX C

DERIVATION OF STEADY-STATE TOTAL FLOW INCIDENCE ANGLE AT RESONANCE

If small perturbations, constant velocity, constant roll rate, and combined asymmetry effects (terms with subscript o) are assumed, the equations of motion for a rolling missile are (ref. 2):

$$\left.\begin{aligned} mu(\dot{\beta} + \dot{\psi} - \alpha\dot{\phi}) &= F_{Y_\beta}\beta + F_{Y,o} \\ mu(\dot{\alpha} + \beta\dot{\phi} - \dot{\theta}) &= -F_{N_\alpha}\alpha - F_{N,o} \\ I\ddot{\theta} - (I - I_X)\dot{\phi}\dot{\psi} &= M_{Y_\alpha}\alpha + M_{Y_q}q + M_{Y,o} \\ I\ddot{\psi} + (I - I_X)\dot{\phi}\dot{\theta} &= M_{Z_\beta}\beta + M_{Z_r}r + M_{Z,o} \end{aligned}\right\} \tag{C1}$$

If $\eta = \beta + i\alpha$, $\Omega = q + ir$, $\dot{\phi} = p$, $u = V$, and symmetric aerodynamics are assumed, equations (C1) combine to:

$$\left.\begin{aligned} \dot{\eta} + ip\eta - i\Omega &= -\frac{F_{N_\alpha}}{mV}\eta + \frac{F_{Y,o} - iF_{N,o}}{mV} \\ \dot{\Omega} + ip\left(1 - \frac{I_X}{I}\right)\Omega &= -\frac{i}{I}\left[M_{Y_\alpha}\eta + iM_{Y_q}\Omega - \left(M_{Z,o} - iM_{Y,o}\right)\right] \end{aligned}\right\} \tag{C2}$$

Simultaneous solution of equations (C2) yields the following equation for vehicle motion:

$$\ddot{\eta} + \left[\frac{F_{N_\alpha}}{mV} - \frac{M_{Y_q}}{I} + ip\left(2 - \frac{I_X}{I}\right)\right]\dot{\eta} + \left\{-\frac{M_{Y_\alpha}}{I} - \frac{F_{N_\alpha}}{mV}\frac{M_{Y_q}}{I} - p^2\left(1 - \frac{I_X}{I}\right) + ip\left[\frac{F_{N_\alpha}}{mV}\left(1 - \frac{I_X}{I}\right) - \frac{M_{Y_q}}{I}\right]\right\}\eta$$

$$= -\frac{M_{Z,o} - iM_{Y,o}}{I} + \frac{F_{Y,o} - iF_{N,o}}{mV}\left[ip\left(1 - \frac{I_X}{I}\right) - \frac{M_{Y_q}}{I}\right] \tag{C3}$$

When steady-state conditions are assumed - that is, $\ddot{\eta}$ and $\dot{\eta}$ equal to zero - the resultant flow incidence angle is as follows:

$$\eta = \frac{-\frac{M_{Z,o} - iM_{Y,o}}{I} + \frac{F_{Y,o} - iF_{N,o}}{mV}\left[ip\left(1 - \frac{I_X}{I}\right) - \frac{M_{Y_q}}{I}\right]}{-\frac{M_{Y_\alpha}}{I} - \frac{F_{N_\alpha}}{mV}\frac{M_{Y_q}}{I} - p^2\left(1 - \frac{I_X}{I}\right) + ip\left[\frac{F_{N_\alpha}}{mV}\left(1 - \frac{I_X}{I}\right) - \frac{M_{Y_q}}{I}\right]} \tag{C4}$$

Since the force term

$$\left(\frac{F_{Y,o} - iF_{N,o}}{mV}\right)\left[ip\left(1 - \frac{I_X}{I}\right) - \frac{M_{Y_q}}{I}\right]$$

is usually negligible in comparison to the moment term

$$\frac{M_{Z,o} - iM_{Y,o}}{I}$$

the resultant flow incidence angle with p equal to some value of ω may be expressed as follows:

$$\eta_{p=\omega} = \eta_{p=0}\left\{\frac{-\frac{M_{Y_\alpha}}{I} - \frac{F_{N_\alpha}}{mV}\frac{M_{Y_q}}{I}}{-\frac{M_{Y_\alpha}}{I} - \frac{F_{N_\alpha}}{mV}\frac{M_{Y_q}}{I} - \omega^2\left(1 - \frac{I_X}{I}\right) + i\omega\left[\frac{F_{N_\alpha}}{mV}\left(1 - \frac{I_X}{I}\right) - \frac{M_{Y_q}}{I}\right]}\right\} \tag{C5}$$

Assumption of negligible $\frac{I_X}{I}$ and $\frac{F_{N_\alpha}}{mV}\frac{M_{Y_q}}{I}$ terms, along with approximate pitch-roll resonance conditions $p = \omega = \left(-\frac{M_{Y_\alpha}}{I}\right)^{1/2}$, allows equation (C5) to be reduced to the following form:

$$\left|\frac{\eta_{p=\omega}}{\eta_{p=0}}\right| = \frac{\left(-\frac{M_{Y_\alpha}}{I}\right)^{1/2}}{\frac{F_{N_\alpha}}{mV} - \frac{M_{Y_q}}{I}} \tag{C6}$$

REFERENCES

1. Enkenhus, K. R., and Bilodeau, P.: Tests on Resonating Models in the C.A.R.D.E. Aeroballistics Range. CARDE Tech. Memo. 158/58, Defense Res. Board (Canada), Feb. 28, 1958. (Available from ASTIA as AD No. 201 256.)

2. Nelson, Robert L.: The Motions of Rolling Symmetrical Missiles Referred to a Body-Axis System. NACA TN 3737, 1956.

3. Crabill, N. L.: Ascent Problems of Sounding Rockets. Rep. 391, AGARD, North Atlantic Treaty Organization (Paris), July 1961.

4. James, Robert L., Jr. (with Appendix B by Norman L. Crabill): A Three-Dimensional Trajectory Simulation Using Six Degrees of Freedom with Arbitrary Wind. NASA TN D-641, 1961.

5. Strass, H. Kurt, and Marley, Edward T.: Rolling Effectiveness of All-Movable Wings at Small Angles of Incidence at Mach Numbers From 0.6 to 1.6. NACA RM L51H03, 1951.

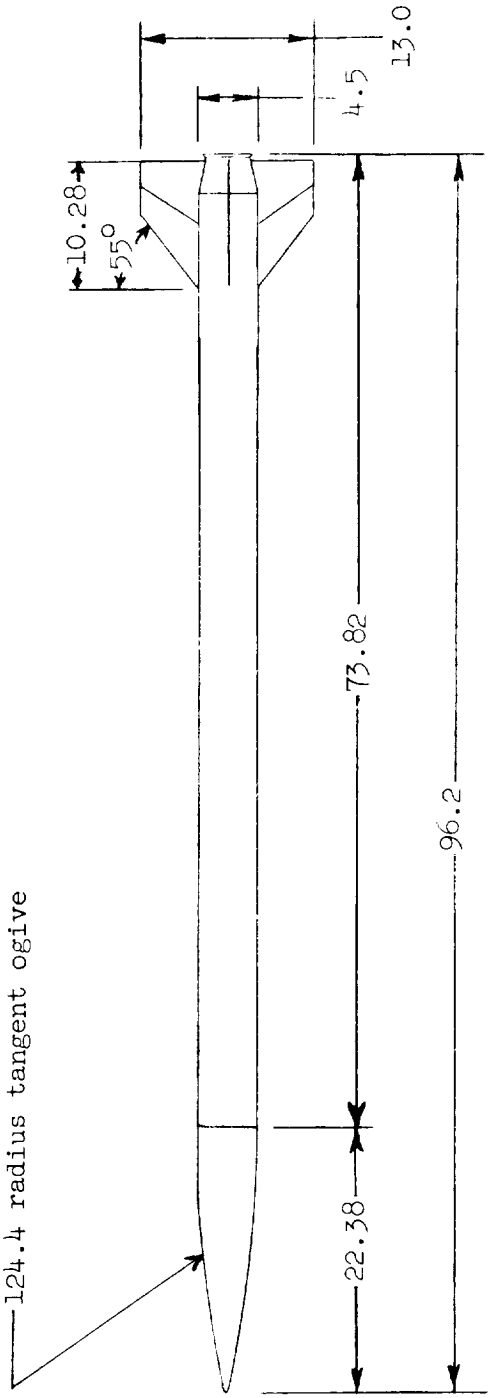

Figure 1.- General external configuration. Dimensions are in inches.

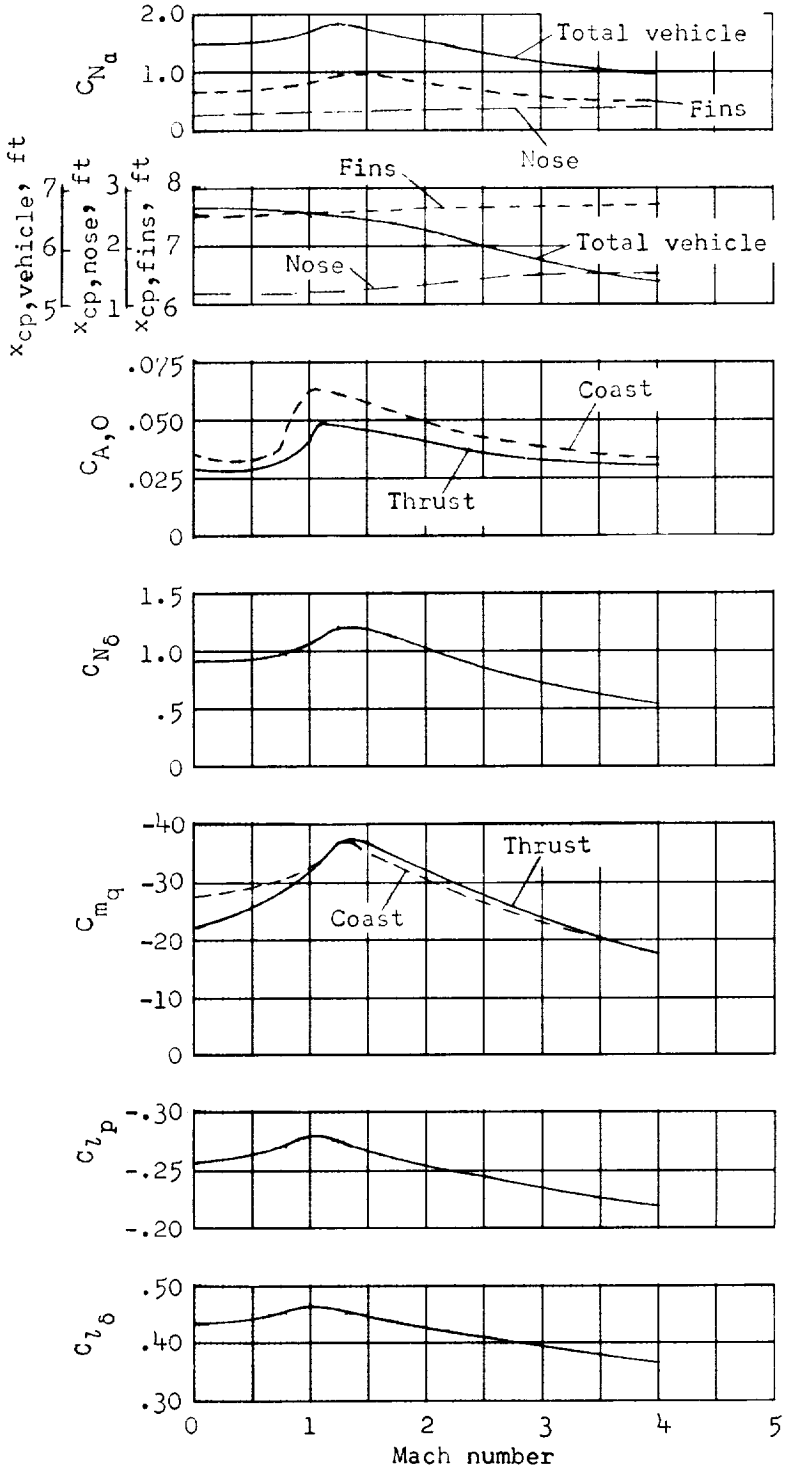

Figure 2.- Estimated values of model aerodynamic parameters. (Reference area and diameter are equal to 1.0.)

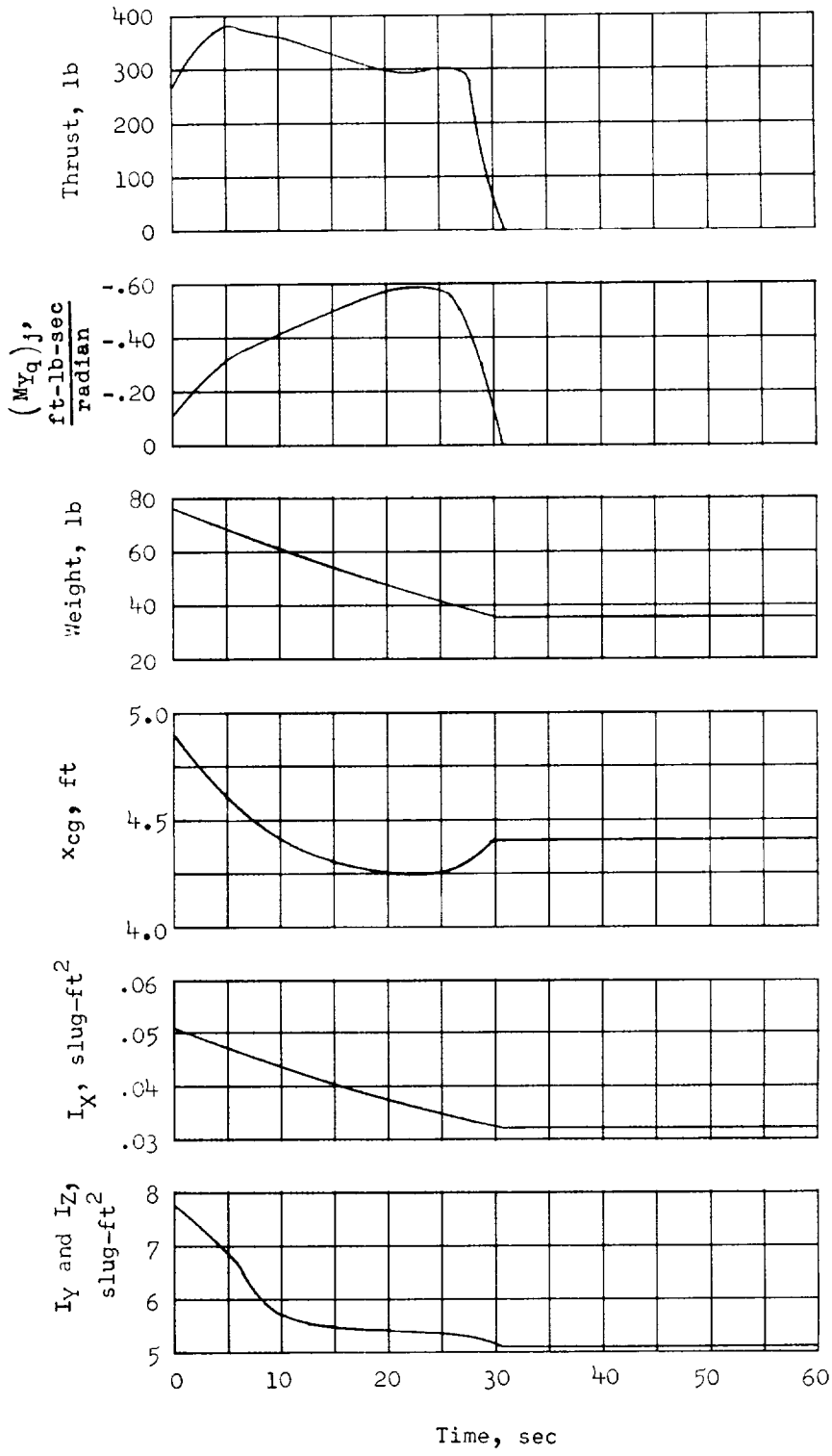

Figure 3.- Estimated physical properties of model.

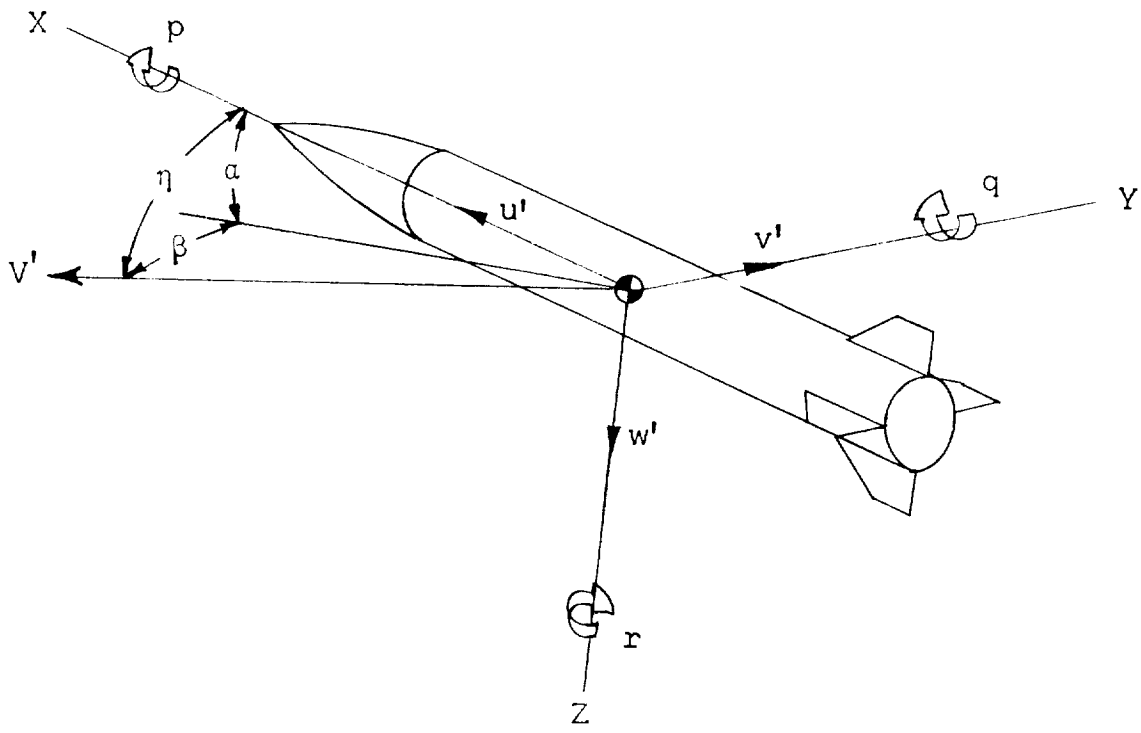

Figure 4.- Vehicle axes system and aerodynamic angles.

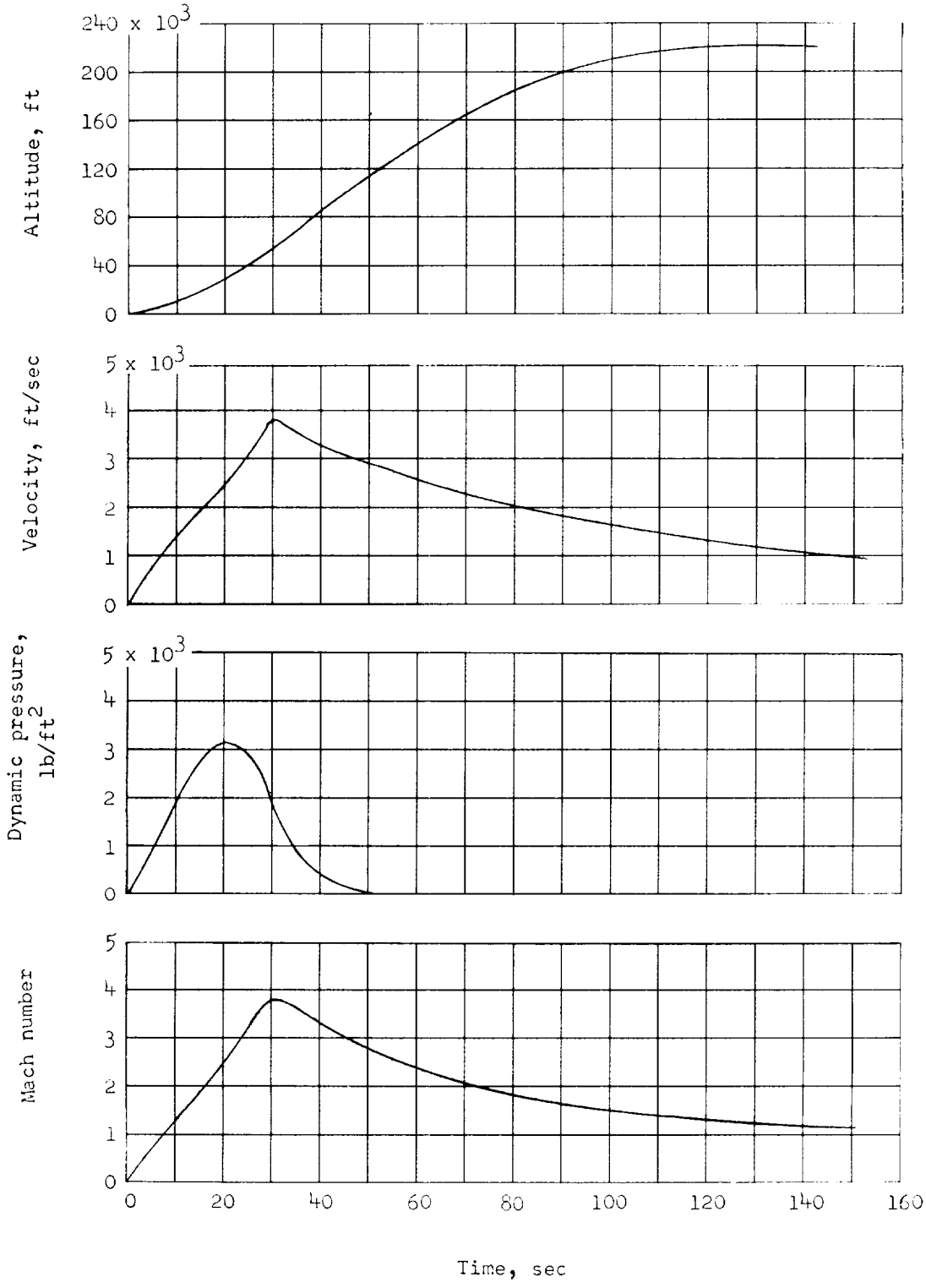

Figure 5.- Vehicle performance characteristics.

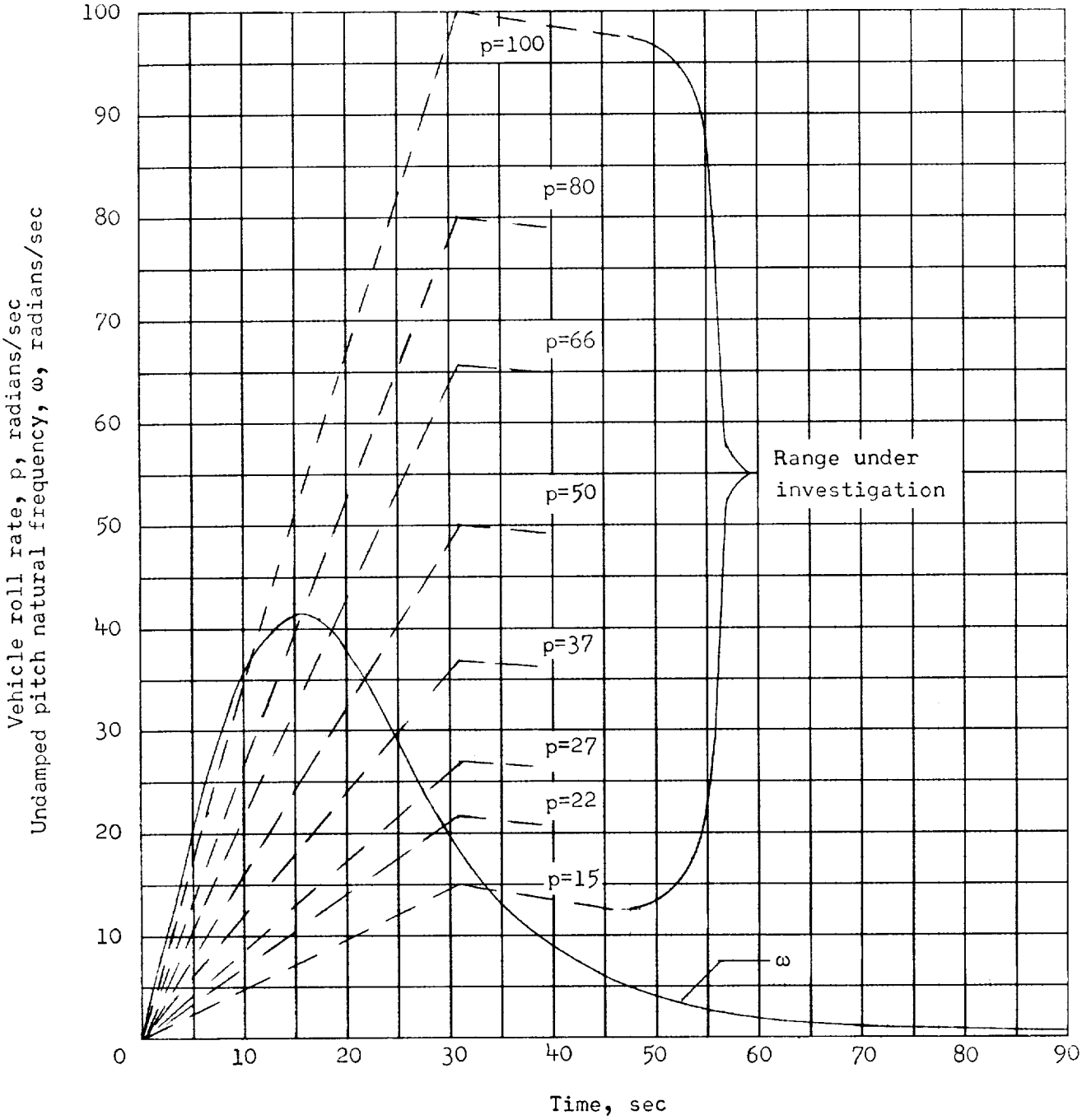

Figure 6.- Undamped pitch natural frequency and vehicle roll rate plotted against time.

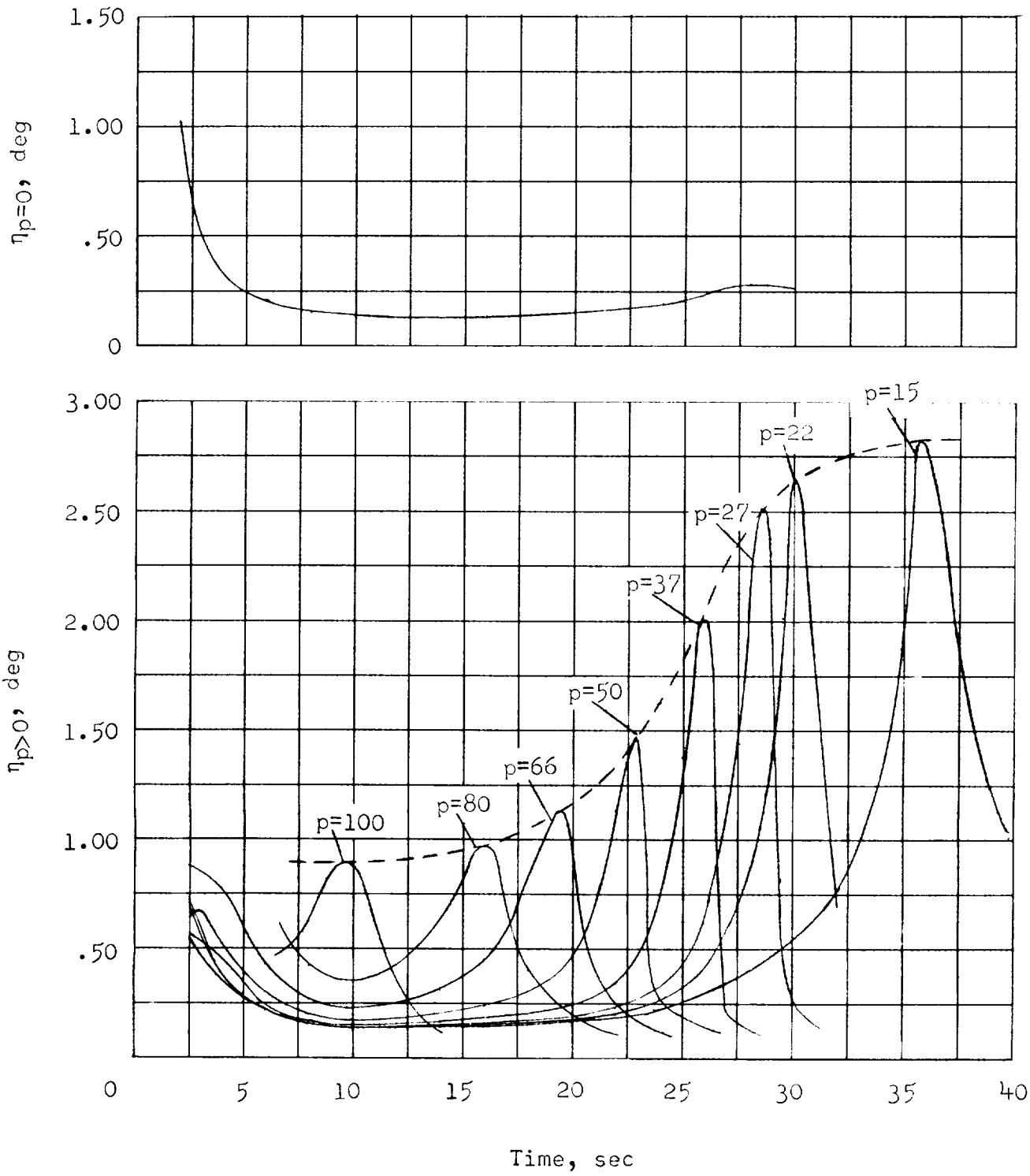

Figure 7.- Resultant flow incidence angle η plotted against time.

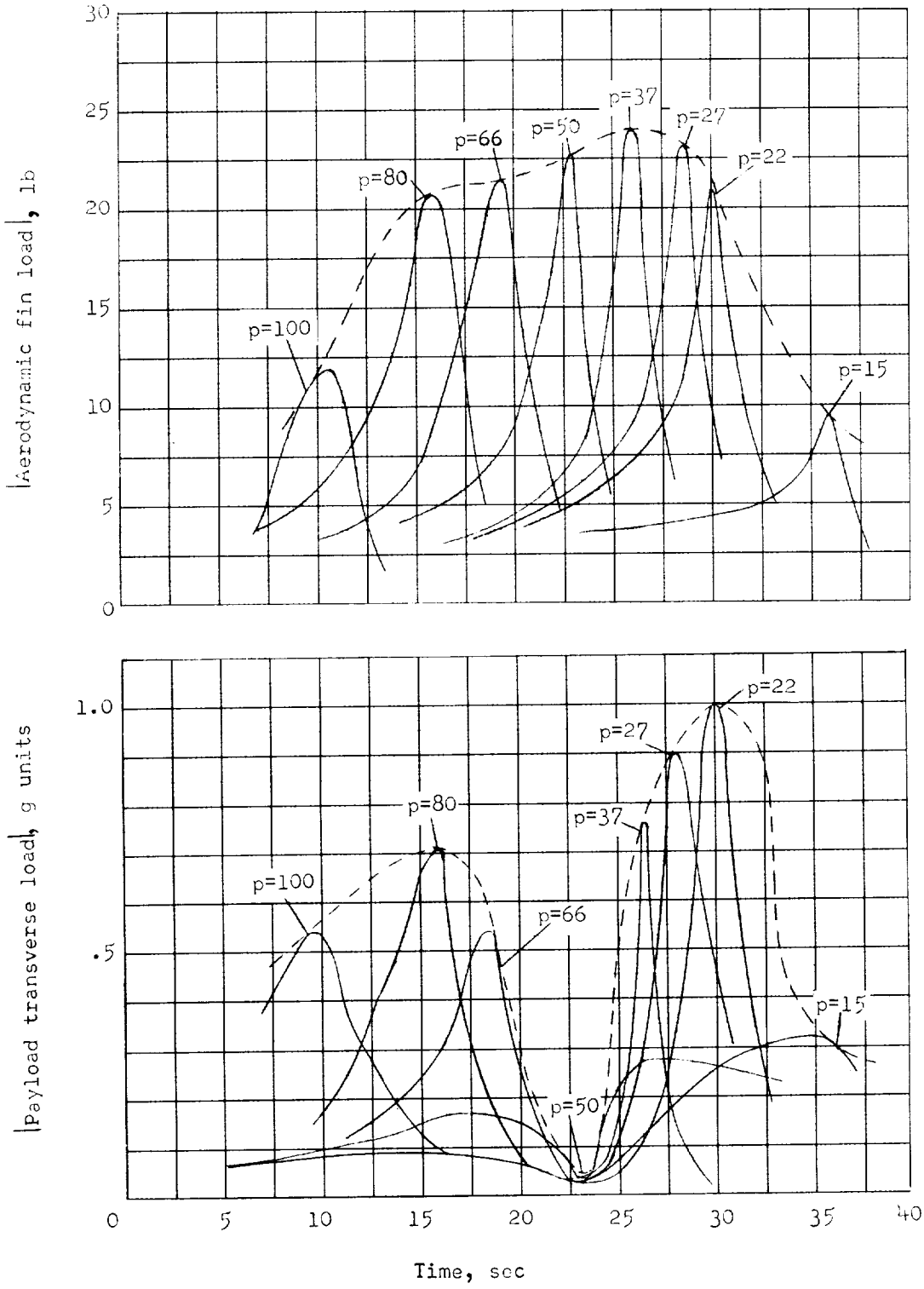

Figure 8.- Principal vehicle loadings plotted against time. Fin load is per fin.

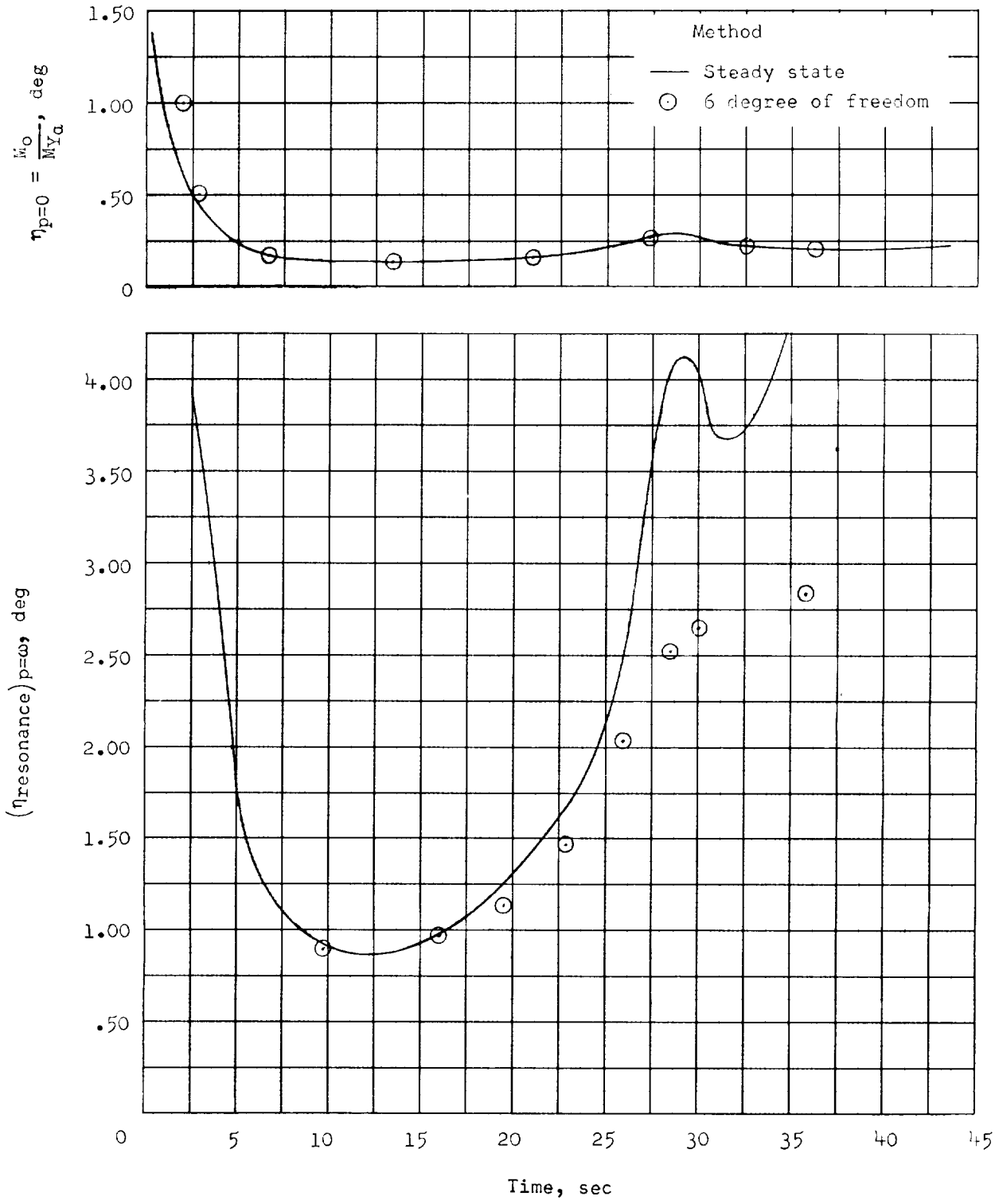

Figure 9.- Resultant flow incidence angle η plotted against time.

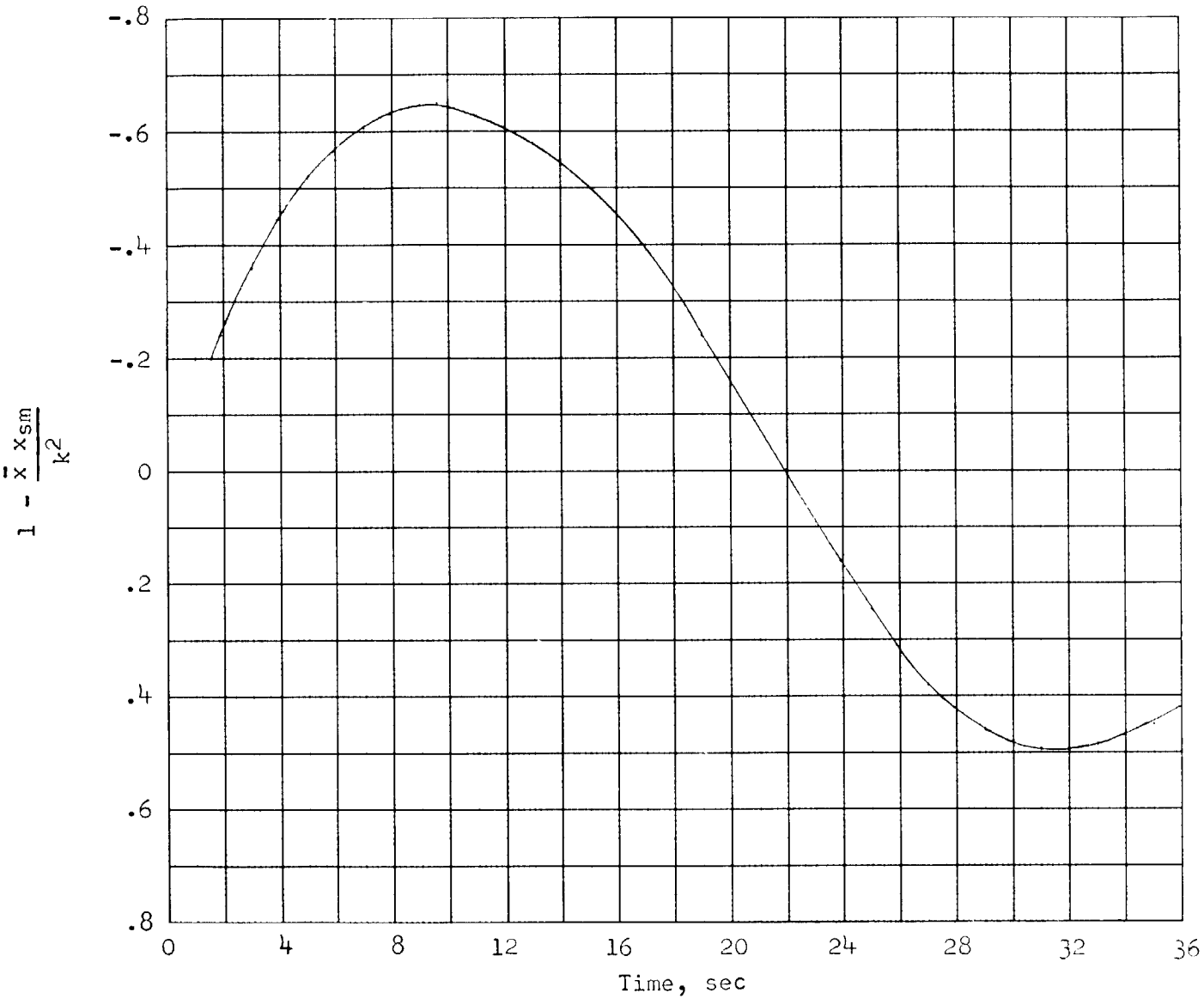

Figure 10.- $1 - \frac{\bar{x}x_{sm}}{k^2}$ plotted against time.

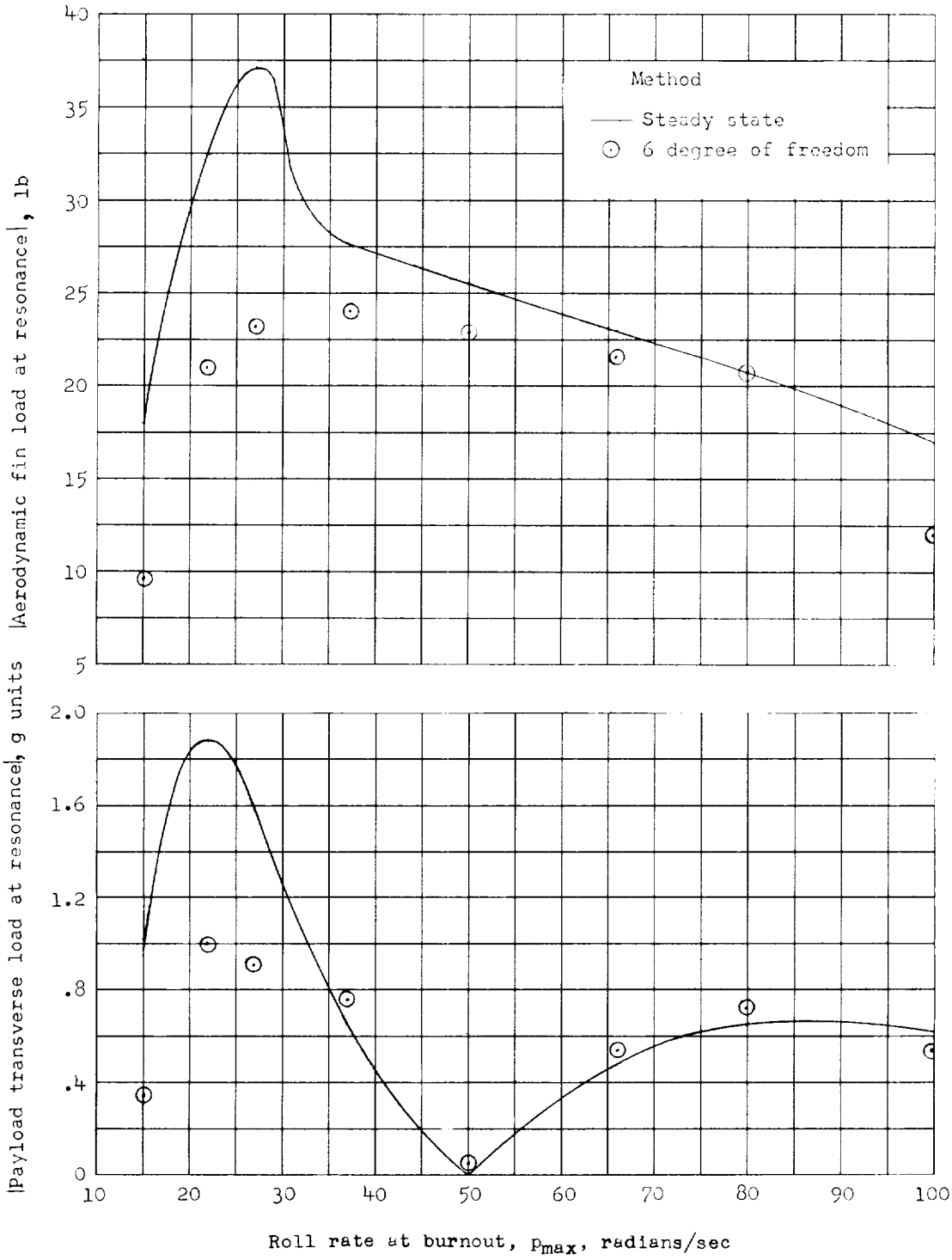

Figure 11.- Principal vehicle loadings at resonance plotted against maximum roll rate. Fin load is per fin.